Low-energy excitations of the Hubbard model on the Kagomé lattice

Yoshiki Imai* and Norio Kawakami
Department of Applied Physics, Osaka University, Suita, Osaka 565-0871, Japan

Hirokazu Tsunetsugu
Yukawa Institute for Theoretical Physics, Kyoto University, Kyoto 606-8502, Japan

(Received 3 May 2003; revised manuscript received 18 August 2003; published 5 November 2003)

The Hubbard model on the Kagomé lattice is investigated in a metallic phase at half filling. By introducing anisotropic electron hopping on the lattice, we control geometrical frustration and clarify how the lattice geometry affects physical properties. By means of the fluctuation exchange approximation, we calculate the spin and charge susceptibilities, the one-particle spectral function, the quasiparticle renormalization factor, and the Fermi velocity. It is found that geometrical frustration of the Kagomé lattice suppresses the instability to various ordered states through the strong reduction of the wave-vector dependence of susceptibilities, thereby stabilizing the formation of quasiparticles due to the almost isotropic spin fluctuations in the Brillouin zone. These characteristic properties are discussed in connection with the effects of geometrical frustration in the strong-coupling regime.

DOI: 10.1103/PhysRevB.68.195103 PACS number(s): 71.10.−w, 71.27.+a

I. INTRODUCTION

Geometrically frustrated metallic systems have attracted much interest since the discovery of the heavy fermion behavior in the transition-metal oxide LiV_2O_4.[1,2] This compound has the spinel structure and the band calculations show that the conduction bands are essentially composed of vanadium $3d$ orbitals, which are well separated from the oxygen $2p$ bands. Therefore when low-energy properties are concerned, it is sufficient to consider only the vanadium $3d$ orbitals.[3–6] The vanadium sublattice in the spinel structure constitutes a network of corner-sharing tetrahedra, i.e., the pyrochlore lattice, and this is a typical example of geometrically frustrated three dimensional (3D) lattices. Various works have revealed unusual low-energy properties of spin systems on the pyrochlore lattice, including the presence of thermodynamic degeneracy of the ground states.[7–13] Another metallic pyrochlore compound $Y(Sc)Mn_2$ also exhibits the heavy fermion behavior where an unusual feature has been observed in the dynamical susceptibility.[14,15] In both compounds, no long-range order has been observed and the specific-heat coefficient is strongly enhanced at low temperatures, similar to the lanthanide or actinide heavy-fermion systems.

The heavy-fermion behavior in the lanthanide or actinide systems is, as well known, attributed to the Kondo effect and the presence of localized f orbital is essential to this mechanism.[16] However, in these transition-metal heavy-fermion systems, $3d$ electrons are much more mobile than f electrons and the presence of local magnetic moment has not been detected so far. It is highly nontrivial whether the enormous mass enhancement is also attributed to the Kondo effect, and there may exist another mechanism leading to the heavy fermionlike behavior. This indeed gives rise to a number of theoretical proposals on the mechanism of the formation of heavy quasiparticles. Among them, it has been claimed that geometrical frustration plays an important role even in the metallic phase when the electron interactions are sufficiently large.[17–28]

The two-dimensional (2D) Kagomé lattice is another geometrically frustrated system, which may be regarded as a 2D analog of the pyrochlore lattice. Antiferromagnetic spin systems on this lattice have been intensively studied and many unusual properties have been found. For example, in the $S=1/2$ Heisenberg antiferromagnet, there exists a finite energy gap between the singlet ground state and triplet excitations, and a thermodynamic number of singlet excitations exist within the singlet-triplet gap due to strong frustration.[29–33] This level scheme of excitations is in common with that for the spin systems on the 3D pyrochlore lattice, and it may be quite generic in geometrically frustrated systems. If electrons become itinerant, electron motion will be coupled to both spin-triplet and spin-singlet excitations. Therefore, quasiparticles in this case may be renormalized in a different manner than other more conventional cases without frustration. To study this issue, we will investigate the correlation effects in the 2D Kagomé lattice. The Kagomé lattice is simpler than the pyrochlore lattice due to the low dimensionality, but otherwise its magnetic properties in the insulating phase are in common with those in the pyrochlore lattice. Therefore, the study on a metallic Kagomé system is a good starting point to investigate how geometrical frustration affects physical properties in a metallic phase, and we expect that many of the results will hold in other frustrated systems including the pyrochlore system.

In this paper, we will investigate the effects of geometrical frustration of the Kagomé lattice on physical properties. In particular, we focus on the possibility of magnetic instability and its relationship to the nature of quasiparticles in a metallic phase. We employ the fluctuation exchange (FLEX) approximation[36–41] for electron correlations and calculate the spin and charge susceptibilities, and the one-particle spectral function. We will show that geometrical frustration of the Kagomé lattice indeed suppresses the instability to various ordered states and stabilizes the formation of quasiparticles.

 ©2003 The American Physical Society

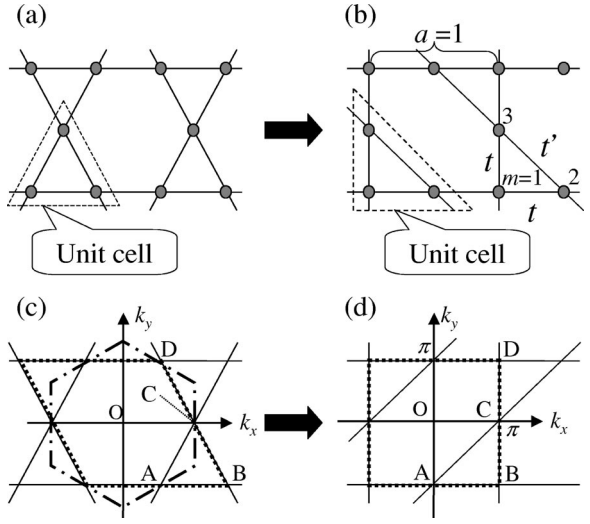

FIG. 1. (a) Original Kagomé lattice and (b) decorated square lattice which is topologically equivalent to (a). Lattice points labeled by $m=1$, 2, and 3 represent relative positions in each unit cell. t and t' are hopping integrals. (c) and (d) BZ of the original Kagomé and decorated square lattices, respectively. A–D represent the corresponding wave vectors in both lattices. Hexagon shown by dash-dotted line in (c) is the first BZ of the Kagomé lattice, which is equivalent to the diamond shown by dotted line. Square shown by dotted line in (d) represents the first BZ corresponding to the diamond in (c).

This paper is organized as follows. In the following section, the model and the method are described briefly, and we show the obtained results in Sec. III. A brief summary is given in Sec. IV.

II. MODEL AND METHOD

The original Kagomé lattice is schematically shown in Fig. 1(a), which is given by a corner-sharing 2D network of triangles. This is topologically equivalent to the decorated square lattice with specific diagonal bonds, as shown in Fig. 1(b), where the unit cell contains three sites. In the following discussions we will deal with the latter lattice, which makes the analysis simpler, since its Brillouin zone (BZ) changes from hexagon [Fig. 1(c)] to square, $-\pi/a<k_x,k_y<\pi/a$ [Fig. 1(d)], where a is the lattice constant. In order to control geometrical frustration on the Kagomé lattice, we here introduce anisotropic hopping, t and t', between nearest-neighbor sites as shown in Fig. 1(b). When $t'/t=1.0$, the system is equivalent to the original Kagomé lattice. The advantage of introducing this anisotropy is that it properly interpolates the nonfrustrated lattice (small t'/t) to the fully frustrated lattice ($t'/t=1$) in the strong-coupling limit $U/t\to\infty$ at half filling, where the system is reduced to the antiferromagnetic Heisenberg model. We expect that the effects due to the frustrated lattice geometry should show up even at weak or intermediate values of U/t. Hereafter, we call the decorated square lattice with $t'/t=1.0$ ($t'/t\neq 1.0$) *isotropic Kagomé* (*anisotropic Kagomé*) lattice and the lattice constant a is taken to be unity, $a=1$.

Then we consider the Hubbard model on the isotropic/anisotropic Kagomé lattice of Fig. 1(b). The Hamiltonian is given by

$$H=\sum_{\mathbf{k},m,m',\sigma}\epsilon_{\mathbf{k}}^{mm'}c_{\mathbf{k}m\sigma}^{\dagger}c_{\mathbf{k}m'\sigma}-\mu\sum_{\mathbf{k},m,\sigma}c_{\mathbf{k}m\sigma}^{\dagger}c_{\mathbf{k}m\sigma}+U\sum_{i,m}c_{im\uparrow}^{\dagger}c_{im\uparrow}c_{im\downarrow}^{\dagger}c_{im\downarrow}, \tag{1}$$

where $c_{\mathbf{k}m\sigma}$ ($c_{\mathbf{k}m\sigma}^{\dagger}$) represents the annihilation (creation) operator of an electron at wave vector $\mathbf{k}$ with site index m and spin σ. Note that the lattice points are labeled by the position of each unit cell i together with the relative position m ($=1,2,3$) in the cell, there exist three bands. Here μ is the chemical potential and U is the on-site Coulomb repulsion. The kinetic energy $\epsilon_{\mathbf{k}}^{mm'}$ is given in the matrix form,

$$\hat{\epsilon}_{\mathbf{k}}=\begin{pmatrix} 0 & -2t\cos\left(\frac{k_x}{2}\right) & -2t\cos\left(\frac{k_y}{2}\right) \\ -2t\cos\left(\frac{k_x}{2}\right) & 0 & -2t'\cos\left(\frac{k_x-k_y}{2}\right) \\ -2t\cos\left(\frac{k_y}{2}\right) & -2t'\cos\left(\frac{k_x-k_y}{2}\right) & 0 \end{pmatrix}. \tag{2}$$

In the following discussions, one hopping integral is fixed and taken as units of energy, $t=1$. In the present study, we focus on the half-filling case, in which geometrical frustration in the strong-coupling regime is most prominent and discuss how the system changes its characteristic properties from the weak coupling to the strong-coupling regime.

In order to study electron correlations in the model, we employ the FLEX approximation, which is a self-consistent perturbation method with respect to the Coulomb interaction U. The FLEX approximation is a conserving approximation based on the idea of Baym and Kadanoff,[34,35] and has been successfully used to describe electron correlations in the high-T_c cuprates and other correlated electron systems.[36–41] In our three-band system, it is convenient to represent

Green's function $\hat{G}$ and the effective interaction $\hat{V}$ in the 3×3 matrix form corresponding to three sites in the unit cell. As far as there is no spin order, the Green's function and other quantities are diagonal in spin space, and we drop the spin index. The self-energy within the FLEX approximation is written as

$$\hat{\Sigma}(k)=\frac{T}{N'}\sum_{q}\ {}^{t}\hat{V}(-q)\hat{G}(k+q), \tag{3}$$

where T is the temperature, $k\equiv(\mathbf{k},i\omega_n)$, and $q\equiv(\mathbf{q},i\nu_l)$, with $\omega_n=(2n-1)\pi T$ and $\nu_l=2l\pi T$, and $N'=N/3$ is the number of total unit cells, with N being the number of total sites. The effective interaction is given by

$$\hat{V}(q)=U\hat{I}+U^2\hat{\chi}(q)+\frac{3}{2}U^2\hat{\chi}(q)\{[\hat{I}-U\hat{\chi}(q)]^{-1}-\hat{I}\}$$

$$+\frac{1}{2}U^2\hat{\chi}(q)\{[\hat{I}+U\hat{\chi}(q)]^{-1}-\hat{I}\}, \tag{4}$$

$$\hat{\chi}(q)=\frac{-T}{N'}\sum_{k}\ \hat{G}(k+q)\hat{G}(k), \tag{5}$$

where $\hat{I}$ is the unit matrix. The Dyson equation for the renormalized Green's function reads

$$\hat{G}(k)^{-1}=\hat{g}(k)^{-1}-\hat{\Sigma}(k), \tag{6}$$

where $\hat{g}(k)$ is the bare Green's function defined as

$$\hat{g}(k)=[(i\omega_n+\mu)\hat{I}-\hat{\epsilon}_{\mathbf{k}}]^{-1}. \tag{7}$$

By numerically iterating the procedures of Eqs. (3)–(6), we obtain the renormalized Green's function.

In order to investigate the spin and charge response of the system, we introduce the generalized susceptibility $\hat{\chi}'(q)$, whose element is defined by

$$\chi'_{m_1m_2,m_3m_4}(q)=\int_0^\beta d\tau e^{i\nu_l\tau}\langle\rho_{m_1m_2}(\mathbf{q},\tau)\rho^\dagger_{m_3m_4}(\mathbf{q},0)\rangle, \tag{8}$$

where $\rho_{mm'}(\mathbf{q},\tau)\equiv(1/\sqrt{N'})\Sigma_i e^{i\mathbf{q}\cdot\mathbf{R}_i}c^\dagger_{im}(\tau)c_{im'}(\tau)$ is the generalized polarization at imaginary time τ. $\mathbf{R}_i$ represents the position of the unit cell i. It should be noted that generalized susceptibility $\hat{\chi}'$ is in the 9×9 matrix form and is diagonal for the spin sector. Within the FLEX approximation, the generalized susceptibility is obtained as

$$\chi'_{m_1m_2,m_3m_4}(q)$$

$$=\frac{-T}{N'}\sum_{k}\ G_{m_2m_4}(k+q)G_{m_3m_1}(k)$$

$$\times e^{-i\mathbf{k}\cdot(\mathbf{r}_{m_1}-\mathbf{r}_{m_3})}e^{i(\mathbf{k}+\mathbf{q})\cdot(\mathbf{r}_{m_2}-\mathbf{r}_{m_4})}, \tag{9}$$

where $\mathbf{r}_m$ $(m=1-3)$ is a relative lattice position in each unit cell [Fig. 1(b)]. The spin and charge susceptibilities, $\hat{\chi}^{(s)}$ and $\hat{\chi}^{(c)}$, are the response of spin-triplet and spin-singlet polarizations, respectively, and their matrix element is given by

$$\chi^{(s,c)}_{m_1m_2,m_3m_4}(q)=\{\hat{\chi}'(q)[\hat{I}\mp\hat{U}\hat{\chi}'(q)]^{-1}\}|_{m_1m_2,m_3m_4}, \tag{10}$$

where the $\mp$ sign should read $-$ for the spin and $+$ for the charge susceptibilities, respectively. The element of $\hat{U}$ is

$$U_{m_1m_2,m_3m_4}=U\delta_{m_1,m_2}\delta_{m_3,m_4}\delta_{m_1,m_3}. \tag{11}$$

III. RESULTS

We numerically iterate the above-mentioned procedure of Eqs. (3)–(6) until the calculated $\hat{G}(k)$'s converge within desired accuracy. The summations are efficiently carried out by using the fast Fourier transform with $N'=64^2$ points in the $\mathbf{k}$ summation and 2048 Matsubara frequencies in the ω_n summation.

A. Free-electron properties

We start with the noninteracting case $U/t=0$. By using an orthogonal transformation, the kinetic term of the Hamiltonian is diagonalized at each $\mathbf{k}$. The result for the isotropic case $t'/t=1.0$ is given by

$$E_{\mathbf{k}1,2}=-t\left[1\pm\sqrt{1+8\cos\left(\frac{k_x}{2}\right)\cos\left(\frac{k_y}{2}\right)\cos\left(\frac{k_x-k_y}{2}\right)}\right],$$

$$E_{\mathbf{k}3}=2t, \tag{12}$$

where $+$ and $-$ signs correspond to the lowest band, $E_{\mathbf{k}1}$, and the middle band, $E_{\mathbf{k}2}$, respectively. While the largest eigenvalue forms a flat band over the whole BZ, the lower two dispersive bands are symmetric with respect to $\omega=-1.0$, and touch each other at $\mathbf{k}=\pm(2\pi/3,-2\pi/3)$ with linear dispersions. Let us define the density of states (DOS) including the chemical potential, as $D(\omega)=(1/N)\Sigma_{\mathbf{k},\alpha}1/(\omega+\mu-E_{\mathbf{k}\alpha})$, and they are shown in Fig. 2(a) for several t'. For the isotropic case $t'/t=1.0$, a δ-function peak appears at $\omega\sim1.5$ $(\omega+\mu=2)$ due to the flat band $E_{\mathbf{k}3}$. In the anisotropic case, the dispersion of the three bands is modified, and the main change is that the highest band is now dispersive, leading to the broadening of the δ-function part of the DOS. However, the qualitative change in the DOS around the Fermi level, $\omega=0$, is quite small. Shown in Fig. 2(b) is the Fermi surface for the corresponding cases. When $t'/t=1.0$, the shape of the Fermi surface is most isotropic. Since the lattice structure is transformed, it seems As t' decreases, the Fermi surface is elongated along the $k_y=k_x$ direction, and becomes more anisotropic. Although the Fermi surface seems anisotropic even for the isotropic Kagomé lattice in Fig. 2(b), this is an apparent feature due to the modified coordinate system [Fig. 1(b)], which was introduced for our convenience. For reference, we show in Fig. 2(c) the Fermi surface for the original Kagomé lattice, from which we can indeed see that the Fermi surface is almost isotropic for $t'/t=1.0$ (solid line).

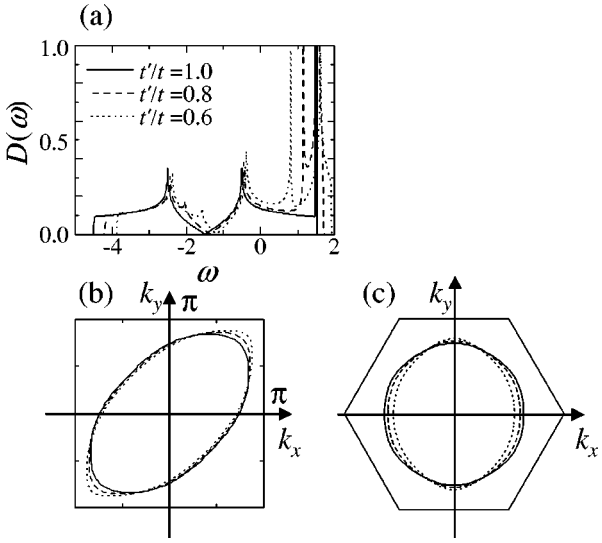

FIG. 2. (a) DOS, and (b) and (c) Fermi surfaces of the *isotropic/anisotropic Kagomé* lattice and the original Kagomé lattice of the noninteracting system ($U/t=0$) at half filling for various hopping amplitude; $t'/t=1.0$ (solid line), 0.8 (dashed line), and 0.6 (dotted line).

Once the free-electron Hamiltonian is diagonalized, it is easy to calculate the susceptibility using Eq. (9). Since the unit cell contains three atoms, there are nine independent modes of polarization concerning the site degrees of freedom in the unit cell, and each of them has both spin-singlet and spin-triplet branches. Correspondingly, the susceptibility is a 9×9 matrix at each $\mathbf{q}$, and its largest eigenvalue is the dominant response. As we are considering the noninteracting case ($U/t=0$) at the moment, the response of spin-singlet polarization is always degenerate with that of spin-triplet polarization. Of course, they start to differ, upon switching on the electron correlations, which will be discussed in a later part. In Fig. 3, we show the largest eigenvalue of the static spin (or charge) susceptibility $\hat{\chi}'(\mathbf{q},0)$ in the Brillouin zone, for the isotropic case $t'/t=1.0$. For the original Kagomé lattice, the susceptibility should have the exact sixfold rotational symmetry in the BZ. However, since in our treatment the original Kagomé lattice is transformed into the topologically equivalent decorated square lattice (*isotropic Kagomé* lattice), the susceptibility has a distorted symmetry. Then the largest values of the susceptibility are located at $\mathbf{q}\approx\pm(0.4\pi,-0.4\pi)$, $\pm(0.4\pi,0.8\pi)$, and $\pm(0.8\pi,0.4\pi)$, and this is due to nesting behavior. Although there is no strong nesting because of the rather isotropic Fermi surface, when the Fermi surface touches itself in a BZ at several points for a given nesting vector, this enhances the susceptibility. Such conditions are illustrated in Fig. 4(a), where the arrows denote the corresponding nesting vectors. It is seen that these vectors indeed give rise to large values of the susceptibility. The results for the anisotropic cases are also shown in the left panels of Fig. 6, and they can also be explained by the Fermi-surface nesting.

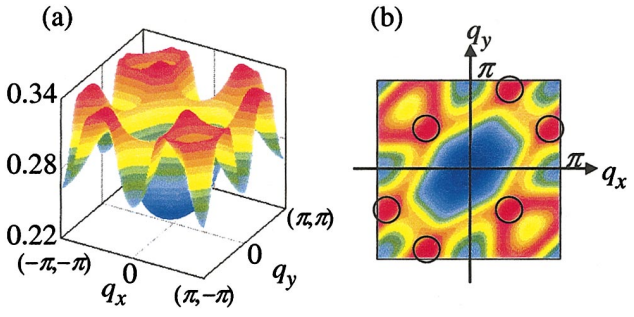

FIG. 3. (Color) (a) Largest eigenvalues of the static susceptibility $\hat{\chi}'(\mathbf{q},0)$ at half filling for $U/t=0$. (b) Contour plot of (a). The circles indicate the location of the peak values. The temperature is $T/t=0.1$.

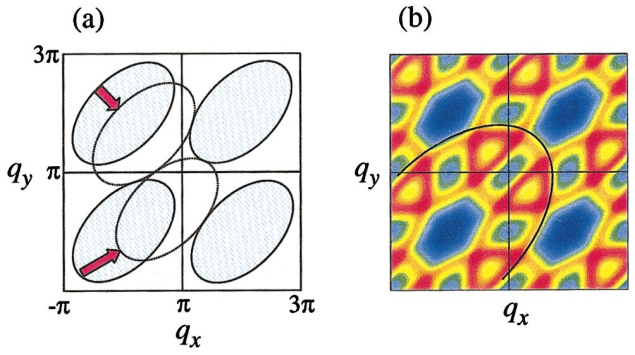

FIG. 4. (Color) (a) Nesting of the Fermi surface. Each solid ellipse depicts the Fermi surface in the extended BZ scheme. Nesting vectors are defined by the shift of the Fermi surface such that the shifted ones (shown by dotted ellipse) touch the original at several $\mathbf{q}$ points. Two examples of the nesting vectors are shown by arrows in the figure. (b) Contour plot of the largest eigenvalues of $\hat{\chi}'(\mathbf{q},0)$. The curve is a guide to eyes.

In the following, we will study the effects of geometrical frustration of the isotropic/anisotropic Kagomé lattice including the Coulomb interaction U. Of course, the strength of electron correlation is characterized by the ratio of the Coulomb interaction to the kinetic energy, but the latter is insensitive to the hopping anisotropy t'/t and therefore the strength is essentially given by the ratio U/t. This is because the change in the total bandwidth and the DOS at the Fermi energy is small. We show the change in the bandwidth as a function of t' in Fig. 5. Although the bandwidth decreases slightly with decreasing hopping t', its change is very small. Even at $t'/t=0$, the total bandwidth is $4\sqrt{2}t\approx5.66t$, which is about 94% of that of the isotropic case ($t'/t=1.0$). This enables us to systematically discuss electron correlations due to U by using the anisotropic model.

B. Magnetic properties

We now turn to study electron correlations in the isotropic/anisotropic Kagomé lattice, and let us start with magnetic properties. Shown in Fig. 6 is the Coulomb interaction dependence of the maximum eigenvalues of the static spin susceptibility $\hat{\chi}^{(s)}(\mathbf{q},0)$ for three typical values of t'. We first discuss the isotropic case ($t'/t=1.0$). For $U/t=0$, the largest values of the susceptibility are located at the six points in the BZ, $\mathbf{q}\approx\pm(0.4\pi,-0.4\pi)$, $\pm(0.4\pi,0.8\pi)$, and

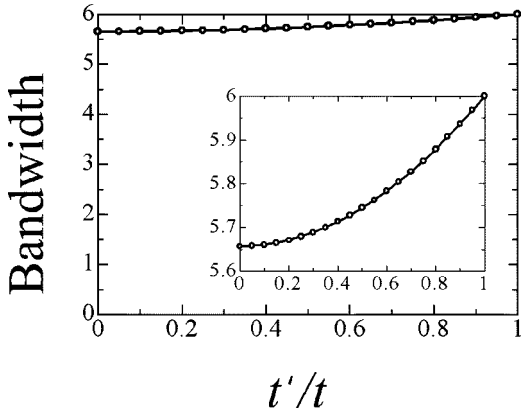

FIG. 5. The t' dependence of the total bandwidth at noninteracting system. The inset shows the magnification.

$\pm(0.8\pi,0.4\pi)$. With increasing U, the susceptibility is enhanced in the whole BZ. However, its **q** dependence is reduced in contrast to the unfrustrated cases. In particular, it is found that the susceptibility for various **q**'s besides the above-mentioned six points are also strongly enhanced with increasing U, so that the **q** dependence of the spin susceptibility is weakened and spin fluctuations become more isotropic in the BZ. We also show the susceptibility for anisotropic cases $t'/t=0.8$ and 0.6 in Fig. 6. Although the (distorted) sixfold symmetry is lost due to hopping anisotropy, the spin susceptibility at $U/t=0$ still has large values at specific **q** positions, which are also able to be expected by the nesting picture similar to $t'/t=1.0$ case. When we switch on U, the peaks in the **q** dependence at $U/t=0$ gradually grow and this enhancement is more remarkable for smaller t'. For example, for $t'/t=0.6$, the peak positions in the intermediate U region are $\mathbf{q}\sim\pm(0.5\pi,-0.5\pi)$, which implies that the system prefers the spin configuration with the period of twice the original unit cell.

We note here that just at $t'/t=0$, a flat band is located at the Fermi level at half filling. It is known that this gives rise to the so-called flat-band ferromagnetic ground state.[42] The nature of the ferromagnetism in this case has been well studied, so that we do not give detailed discussions for the cases $t'/t\ll 1.0$.

In order to discuss the instability to spin ordered states, it is instructive to compare the FLEX results with those calculated by the random-phase approximation (RPA). Shown in Fig. 7(a) is the inverse of the largest value of the spin susceptibility $\hat{\chi}^{(s)}(\mathbf{q},0)$ within the whole BZ. Note that the corresponding **q**, which gives the largest $\hat{\chi}^{(s)}(\mathbf{q},0)$, changes continuously depending on the Coulomb interaction, temperature, etc. When this value becomes zero, the corresponding spin order, i.e., spin-density wave (SDW), appears. Both results of the FLEX approximation and the RPA show that the dominant spin susceptibility is suppressed with increasing t', indicating the suppression of spin order. Note that the RPA spin susceptibility diverges at a finite U/t for all t', and

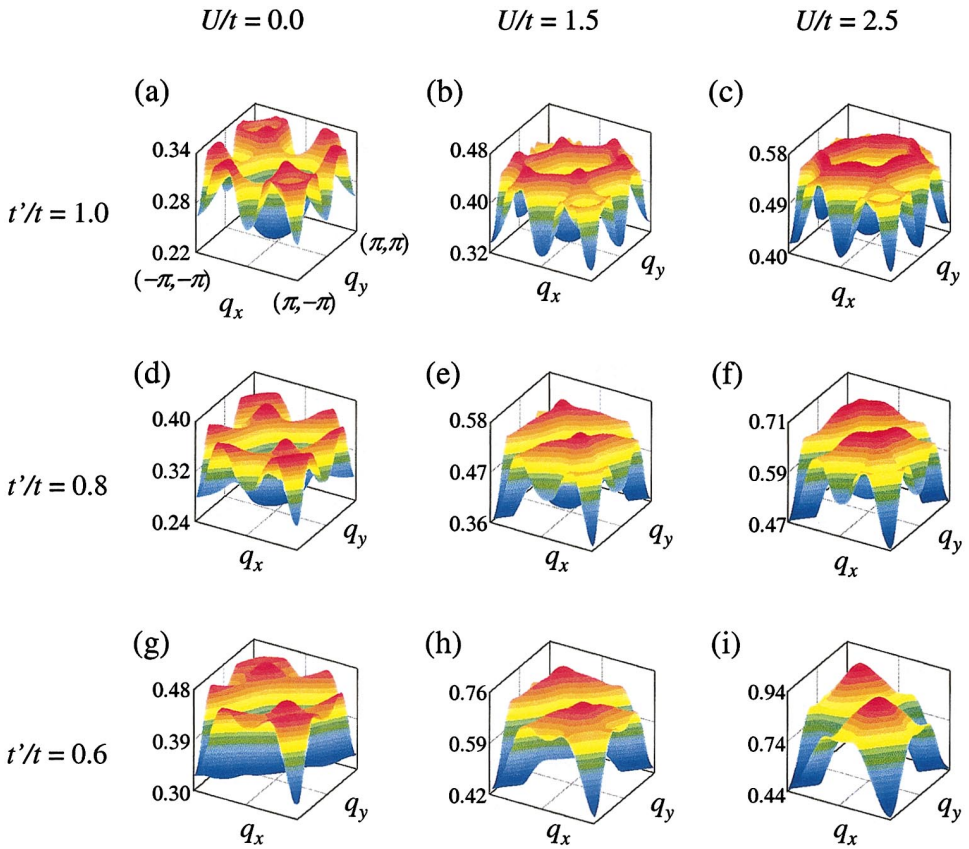

FIG. 6. (Color) The maximum eigenvalues of the static spin susceptibility $\hat{\chi}^{(s)}(\mathbf{q},0)$ for three typical U values. Upper, middle, and lower panels correspond to $t'/t=1.0$, 0.8, and 0.6, respectively. The temperature T/t is 0.1.

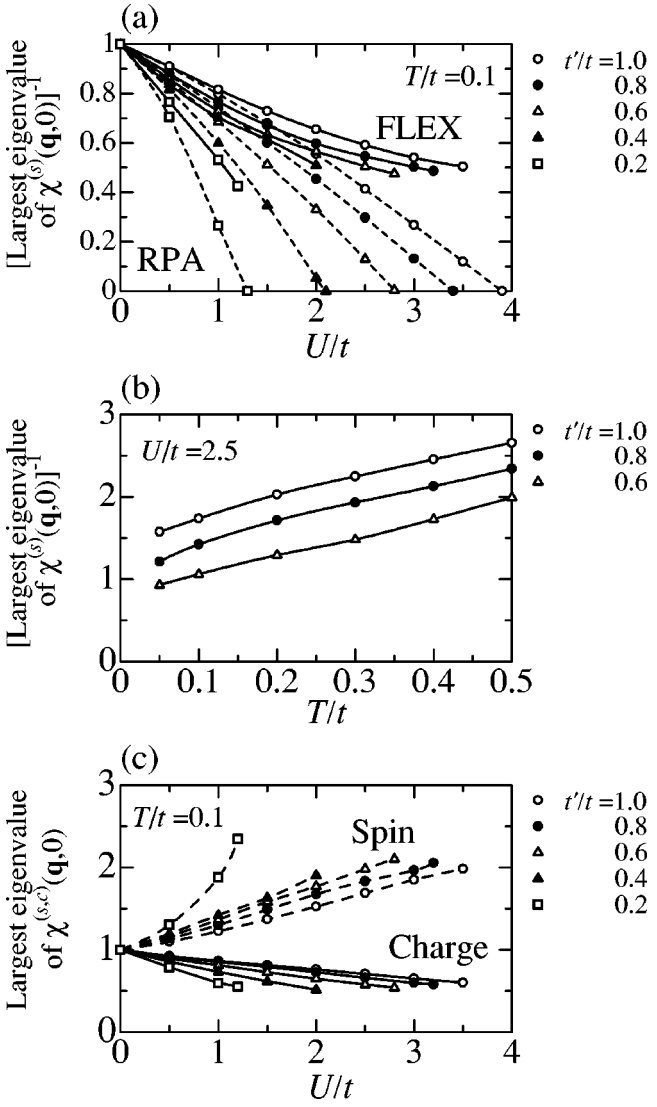

FIG. 7. (a) The inverse of the largest eigenvalue of the spin susceptibility for all **q** in the whole BZ as a function of the Coulomb interaction U for various t'. Solid (dashed) lines represent the results of the FLEX approximation (RPA). (b) The inverse of largest eigenvalues of the spin susceptibility as a function of temperature T/t for several values of t'. U/t is 2.5. (c) Largest eigenvalues of the spin and charge susceptibilities calculated by the FLEX approximation as a function of U/t. Solid (dashed) lines denote the charge (spin) sector, respectively. In both (a) and (c), all of the data are normalized by the value at $U/t=0.0$ and the temperature $T/t=0.1$.

the divergence is even enhanced, as seen in the concave shape of the lines, due to the multiband structure. On the other hand, the enhancement in the FLEX results is much weaker at large U/t and the spin susceptibility does not seem to diverge. The behavior of the FLEX results is more reliable in the intermediate U/t region, since mode-mode couplings are completely neglected in the RPA and the instability is overestimated. In particular, the suppression is most remarkable around the isotropic point $t'\sim t$, and we may conclude that no spin order is realized for the isotropic Kagomé lattice within the FLEX approximation. For reference, the inverse of the largest value of the spin susceptibility is also plotted as a function of temperature in Fig. 7(b). As should be expected, these values are suppressed with decreasing temperature, but remain finite even at low temperatures. Furthermore, as the system approaches the isotropic model with $t'/t\sim 1.0$, the susceptibility becomes smaller in the whole temperature region, indicating that the SDW instability is suppressed for the isotropic model.

Summarizing the magnetic properties, the spin susceptibility is enhanced in the presence of the Coulomb interaction in the whole BZ, but geometrical frustration of the Kagomé lattice has a strong effect to reduce the **q** dependence of the susceptibility and to suppress the instability to any type of the SDW order. Although the present calculations are based on a weak-coupling approach, the obtained results are quite consistent with properties expected in the strong-coupling regime, the frustrated Heisenberg spin system, where the magnetic order is suppressed due to strong frustration.

We have so far discussed the instability of spin-triplet polarization, but the instability in the spin-singlet channel is even weaker. The largest eigenvalues of the charge susceptibility $\hat{\chi}^{(c)}(\mathbf{q},0)$ in the BZ are always smaller than that for $\hat{\chi}^{(s)}(\mathbf{q},0)$ within the FLEX approximation and there is no indication of charge order [charge-density wave (CDW)] or current-carrying state [shown in Fig. 7(c)]. Thus we do not give detailed discussions on the charge susceptibility here.

C. One-particle spectral function

We now discuss the one-particle spectral function and the total spectral density, which are defined by

$$A(\mathbf{k},\omega)=-\frac{1}{3\pi}\sum_{m}\mathrm{Im}G_{mm}(\mathbf{k},\omega+i\delta), \tag{13}$$

$$\rho(\omega)=\frac{1}{N'}\sum_{\mathbf{k}}A(\mathbf{k},\omega), \tag{14}$$

where δ is a small adiabatic constant.

In order to obtain dynamical quantities in the FLEX approximation, the analytic continuation from the imaginary Matsubara frequency to the real frequency is usually performed by using the Padé approximation or the maximum entropy method. However, it is known that this procedure sometimes encounters numerical difficulties. In the present study, we directly calculate the spectral function in a real frequency formulation without resorting to analytic continuation. (Our formulation is similar to those used in the previous works,[37–39] but simpler from the viewpoint of numerical techniques.) We need a small but finite adiabatic constant δ for Green's function, but its effects can be corrected systematically and we have checked that the Padé approximation[43] reproduces similar results. We show here the results calculated by our real frequency technique, since they are free from numerical errors due to analytic continuation.

Figure 8 shows the one-particle spectral function for three distinct wave vectors close to the Fermi surface. Since the shape of Fermi surface changes with t', we have chosen proper wave vectors **k**, which should be closer to the three

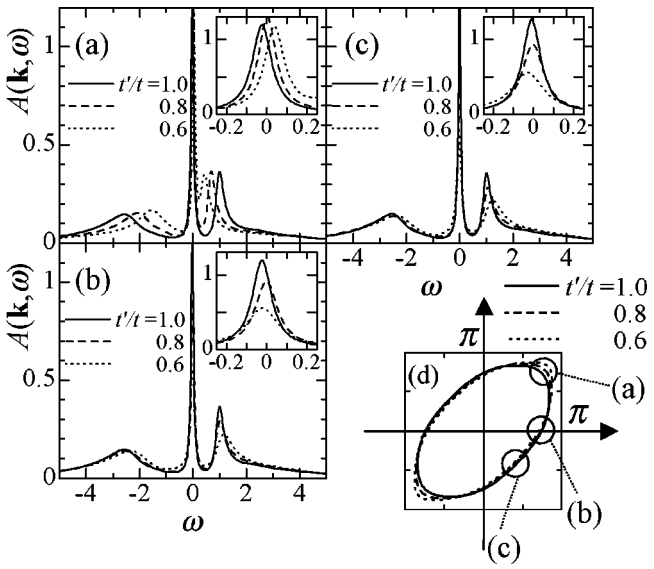

FIG. 8. One-particle spectra for various **k**. (a) $\mathbf{k}\approx(0.75\pi,0.75\pi)$, (b) $\mathbf{k}\approx(0.75\pi,0)$, and (c) $\mathbf{k}\approx(0.42\pi,-0.42\pi)$, respectively. (d) Fermi surface for several values of t'. Small circles represent the location of **k** chosen for (a–c). The energy is measured from the Fermi level ($\omega=0$). The Coulomb repulsion $U/t=2.5$, the temperature $T/t=0.1$, and adiabatic constant $\delta=0.05$. The insets show the magnification of the low-frequency regime.

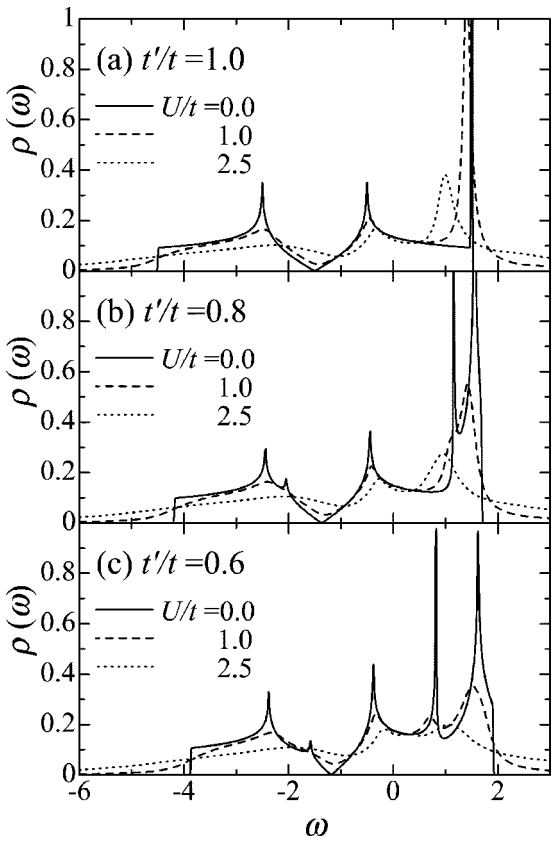

FIG. 9. Total spectral density for various U. (a) $t'/t=1.0$, (b) $t'/t=0.8$, and (c) $t'/t=0.6$.

typical Fermi points listed in the caption. All the spectra shown consist of three peaks reflecting the three-band structure; namely, the αth peak is mainly due to the contribution of the band with $E_{\mathbf{k}\alpha}$. As U increases, two peaks at large $|\omega|$ are gradually smeared due to lifetime effects. On the other hand, the peak near $\omega=0$ keeps a sharp structure, implying a well-defined Fermi-liquid behavior. Note that these peaks are not exactly located at $\omega=0$ due to the discretization of **k** points in the numerical calculations. However, this does not give any essential changes in the following discussions. This behavior is particularly prominent in the isotropic case $t'/t=1.0$ irrespective of **k**'s (a–c). However, in the anisotropic cases of $t'/t=0.8$ and 0.6, the central peak changes its shape from (a) $\mathbf{k}\approx(0.75\pi,0.75\pi)$ to (c) $\mathbf{k}\approx(0.42\pi,-0.42\pi)$, where the amplitude of the spectra at $\omega\sim0$ is reduced with the decrease of t'/t. This behavior suggests that quasiparticles are stabilized in the region of isotropic hopping $t'\sim t$. As discussed in the preceding section, increasing t' represents the enhancement of effects of geometrical frustration, and this leads to the trend that the wave-vector dependences are strongly reduced in the BZ. Since the spin fluctuations are localized in the real space and these amplitude are strongly reduced, various orders, such as the SDW, CDW, and currant-carrying states, are suppressed and the metallic state is stabilized. Therefore the quasiparticle picture becomes fine description. This result indicates that geometrical frustration on the Kagomé lattice may be important for the formation of quasiparticles.

For reference, we also present in Fig. 9 the results of the total spectral density defined by Eq. (14). As U increases, the total spectral density is smeared in the whole energy region due to the lifetime effect. However, in the weak-coupling regime treated here, the total spectral density near the Fermi level is rather insensitive to the change in anisotropic hopping t' in comparison with other physical quantities, such as the one-particle spectra, etc. Although the one-particle spectral weight with **k** for the $k_y=-k_x$ direction close to the Fermi surface is strongly reduced at $\omega\sim0$ with decreasing t'/t, the amplitude of total spectral density at $\omega\sim0$ becomes largest at $t'/t=0.6$ even when U is introduced. In the intermediate U region, the one-particle spectrum at **k** far from the Fermi surface mainly consists of the incoherent parts. Since the local spectral density is obtained by the **k** summation in Eq. (14), the contributions of these incoherent parts far from Fermi surface become quite large even at $\rho(0)$ with increasing U. Therefore, it is difficult to discuss about the coherence of quasiparticles only based on the total spectral density $\rho(0)$, and we need more detailed information from $A(\mathbf{k},\omega)$.

Summarizing this section, as compared with the total spectral density, the one-particle spectrum gives us more detailed information on the nature of quasiparticles. The weight of the coherent part in the one-particle spectrum grows with increasing t', which means that the quasiparticle behavior is stabilized by geometrical frustration.

D. Renormalization effects

To investigate the properties of quasiparticles in more detail, we calculate the renormalization factor and the Fermi

velocity of quasiparticles. According to the conventional Fermi-liquid theory, the one-particle spectrum consists of the δ-function-like coherent part and the broad incoherent part. As the Coulomb interaction increases, the quasiparticle mass is enhanced and the weight of the coherent part becomes small. For the single-band case, the renormalization factor is given by the self-energy as

$$Z_{\mathbf{k}}=\left[1-\left.\frac{\partial \mathrm{Re}\Sigma(\mathbf{k},\omega)}{\partial\omega}\right|_{\omega=0}\right]^{-1}, \tag{15}$$

which corresponds to the weight of the coherent part. However, in the present case, the one-particle spectrum at a given $\mathbf{k}$ has contribution of three bands. When the coherent quasiparticle part is separated from the other parts, it is given by

$$A^{\mathrm{coh}}(\mathbf{k},\omega)=\frac{1}{\pi}\frac{Z_{\mathbf{k}}\gamma}{(\omega-\xi_{\mathbf{k}})^2+\gamma^2}+b, \tag{16}$$

where $\xi_{\mathbf{k}}$ is the shift from the Fermi level, b is the correction due to the other peaks which are located far from the Fermi level, and γ represents the inverse of lifetime of the quasiparticle. These parameters can be determined by numerical fitting of the data of the spectral function. However, instead of performing this procedure, we here use an alternative approach to simply determine the renormalization factor. Since the middle band near the Fermi level is isolated sufficiently far from the other bands, we can introduce the following effective self-energy in the low-energy region:

$$\tilde{\Sigma}^{\mathrm{eff}}(\mathbf{k},\omega)\equiv\tilde{g}(\mathbf{k},\omega)^{-1}-\tilde{G}(\mathbf{k},\omega)^{-1}, \tag{17}$$

where

$$\tilde{g}(\mathbf{k},\omega)=\frac{1}{3}\sum_m g_{mm}(\mathbf{k},\omega), \tag{18}$$

$$\tilde{G}(\mathbf{k},\omega)=\frac{1}{3}\sum_m G_{mm}(\mathbf{k},\omega). \tag{19}$$

The approximate formula for the renormalization factor then reads

$$Z_{\mathbf{k}}=\left[1-\left.\frac{\partial \mathrm{Re}\tilde{\Sigma}^{\mathrm{eff}}(\mathbf{k},\omega)}{\partial\omega}\right|_{\omega=0}\right]^{-1}. \tag{20}$$

Although Eq. (20) is not exact, this formula works well as far as the low-energy regime is concerned. We have checked for several $\mathbf{k}$ that the results obtained by using Eq. (20) are in good agreement with the renormalization factor determined by the fitting Eq. (16).

Figure 10 shows the $\mathbf{k}$ dependence of the renormalization factor as a function of U for various t'. We show the results only in the $\mathbf{k}$ region, $0\leqslant|k_y|\leqslant k_x\leqslant\pi$, because the values in other regions are readily obtained according to the symmetry property. In all the cases of t'/t, the renormalization factor $Z_{\mathbf{k}}$ decreases with the increase of U, meaning that the effective mass is enhanced. An important point is that $Z_{\mathbf{k}}$ becomes nearly independent of $\mathbf{k}$ in the isotropic case ($t'/t=1.0$), being consistent with the results of one-particle spectral

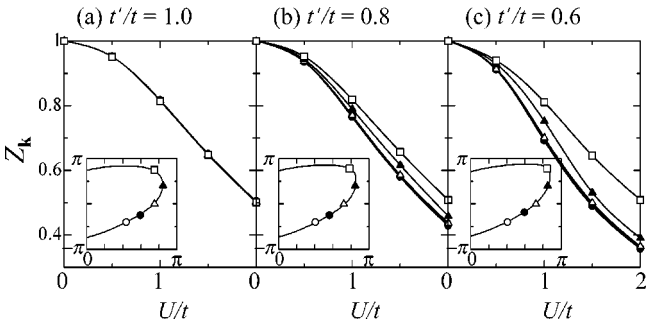

FIG. 10. Renormalization factor as a function of U at temperature $T/t=0.1$; (a) $t'/t=1.0$, (b) $t'/t=0.8$, and (c) $t'/t=0.6$, respectively. The insets show the Fermi surface (solid line) in the half BZ ($0\leqslant k_x\leqslant\pi$) where symbols (open circles, etc.) denote various $\mathbf{k}$ for which $Z_{\mathbf{k}}$ is calculated.

functions. On the other hand, with decreasing t', the difference in $Z_{\mathbf{k}}$ for different $\mathbf{k}$'s becomes more remarkable. In particular, the $Z_{\mathbf{k}}$ for $\mathbf{k}$'s along the direction of $k_y=-k_x$ is strongly renormalized. It should be noted that the largest $Z_{\mathbf{k}}$ in the anisotropic case [open squares in Fig. 10(b) and 10(c)] has almost the same amplitude as that for $t'/t=1.0$. In other words, with decreasing t', the quasiparticle weight is reduced in comparison with that of $t'/t=1.0$. Therefore this is another evidence that geometrical frustration stabilizes the Fermi-liquid behavior up to larger U regime when $t'/t=1.0$ (the isotropic Kagomé lattice).

Shown in Fig. 11 is the absolute value of the Fermi velocity, which is given by

$$|v_{\mathbf{k}}^F|=\sqrt{\left(\frac{\partial\tilde{E}_{\mathbf{k}}}{\partial k_x}\right)^2+\left(\frac{\partial\tilde{E}_{\mathbf{k}}}{\partial k_y}\right)^2}, \tag{21}$$

which is obtained from the renormalized quasiparticle energy of the middle band,

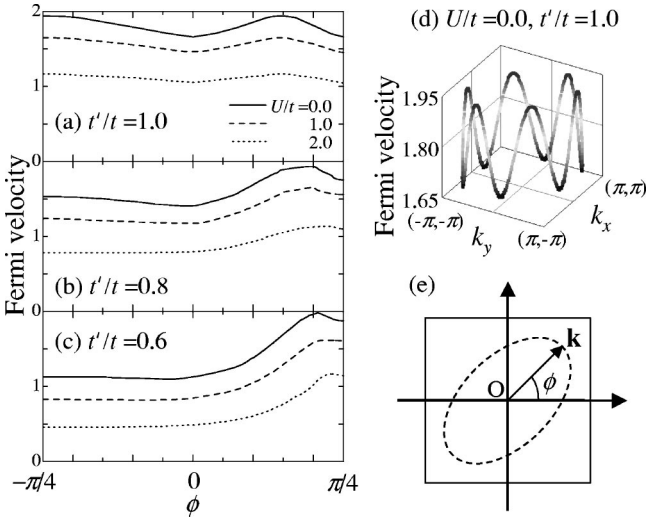

FIG. 11. Angular dependence of the Fermi velocity for various U; (a) $t'/t=1.0$, (b) $t'/t=0.8$, and (c) $t'/t=0.6$ [Eq. (21)]. (d) Fermi velocity at $U/t=0$ and $t'/t=1.0$ in the $\mathbf{k}$ space. (e) Angle ϕ of the $\mathbf{k}$ point on the Fermi surface.

$$\tilde{E}_{\mathbf{k}} = Z_{\mathbf{k}}[E_{\mathbf{k}}^{(2)} - \mu + \mathrm{Re}\tilde{\Sigma}^{\mathrm{eff}}(\mathbf{k},0)]. \quad (22)$$

In the case of $t'/t=1.0$, the Fermi velocity has the distorted sixfold rotational symmetry in the BZ reflecting the lattice structure [Fig. 11(d)] and the ratio of the largest and smallest velocity is about 1.17 for $U/t=0$. With increasing U, the ratio is gradually reduced to the smaller value of about 1.10 for $U/t=2.0$, indicating again the suppression of the **k** dependence. On the other hand, for the anisotropic case $t'/t<1.0$, the ratio is not reduced but enhanced. For instance, for $t'/t=0.6$, the ratio changes from about 1.79 for $U/t=0.0$–2.45 for $U/t=2.0$. These results are in accordance with those of the renormalization factor in the sense that the wave-vector dependence grows with increasing hopping anisotropy.

IV. SUMMARY AND DISCUSSION

In this paper, we have studied how geometrical frustration of the isotropic/anisotropic Kagomé lattice affects physical properties in a metallic phase. By using the FLEX approximation for the Hubbard model at half filling, we have calculated the spin and charge susceptibility, the one-particle spectrum, the total spectral density, the quasiparticle renormalization factor, and the Fermi velocity. In the isotropic Kagomé lattice, we have shown that the spin susceptibility is enhanced by the Coulomb interaction as far as the amplitude of susceptibility is concerned. However, in contrast to ordinary cases of magnetic instability, its wave-vector dependence is strongly suppressed at the same time, and there appear many peaks in the BZ accumulating to form a line. This reduction of the wave-vector dependence around the Fermi surface is also observed for other quantities, such as the quasiparticle weight of the one-particle spectrum. We have demonstrated that this behavior is indeed due to the frustrated lattice geometry by controlling frustration by anisotropic hopping; the **k** dependence is considerably recovered with the decrease of t', i.e., when frustration is reduced. By comparing the spin susceptibility calculated by the FLEX approximation with that of RPA, we have shown that the instability to magnetically ordered phases is dramatically suppressed by mode-mode couplings of fluctuations, which are neglected in the RPA level. This suppression is most prominent in the isotropic case, i.e., most frustrated case. Furthermore, considering the one-particle spectrum, we have shown that the coherent part has a large weight in the isotropic Kagomé lattice up to larger U regime, which is also consistent with the behaviors of the renormalization factor and Fermi velocity. These results indicate that geometrical frustration stabilizes the formation of quasiparticles.

The main conclusion of the present study is that the strong geometrical frustration reduces the wave-vector dependence of spin fluctuations and suppresses the instabilities to various orders, such as the SDW, CDW, and current-carrying states, so that the Fermi-liquid behavior is stabilized and the quasiparticles become well defined in the isotropic Kagomé lattice. This conclusion is derived from the FLEX approximation, which is an essentially weak-coupling approach, but it is consistent with the results known for the strong-coupling model, i.e., the absence of any magnetic order due to strong frustration in the antiferromagnetic spin system on the Kagomé lattice. Therefore, it is reasonable that characteristic properties discussed in the present work for the weak-coupling Hubbard model on the Kagomé lattice are naturally connected to those inherent in the frustrated Heisenberg spin system.

Within the FLEX approximation in this paper, we have not observed other ordered states, either such as the staggered flux (current-carrying) state[44–46] and the charge ordered state[47] etc., which are other possible orders in the strong-coupling regime. In the present case of half filling, although charge ordered states are unlikely, a staggered flux state may appear due to strong geometrical frustration. Furthermore, upon finite hole doping, geometrical frustration may realize a charge ordered state. It is an interesting open problem to be addressed in the future.

Experimentally, most compounds studied so far have been restricted to spin systems on the Kagomé lattice, such as $SrCr_8Ga_4O_{19}$.[48,49] It is thus interesting to study electron correlations in metallic Kagomé lattice materials.

ACKNOWLEDGMENTS

One of the authors (Y.I.) would like to acknowledge helpful discussion with T. Takimoto. The work was partly supported by a Grant-in-Aid from the Ministry of Education, Science, Sports, and Culture of Japan. A part of the numerical calculations was performed on computers at the supercomputer center at the Institute for the Solid State Physics, The University of Tokyo, and at Yukawa Institute Computer Facility, Kyoto University.

*Present address: PRESTO, Japan Science and Technology Corporation (JST), *c/o* Institute for Solid State Physics, University of Tokyo, Kashiwanoha 5-1-5, Chiba, Japan. Email address: imai@issp.u-tokyo.ac.jp

[1] S. Kondo, D.C. Johnston, C.A. Swenson, F. Borsa, A.V. Mahajan, L.L. Miller, T. Gu, A.I. Goldman, M.B. Maple, D.A. Gajewski, E.J. Freeman, N.R. Dilley, R.P. Dickey, J. Merrin, K. Kojima, G.M. Luke, Y.J. Uemura, O. Chmaissem, and J.D. Jorgensen, Phys. Rev. Lett. **78**, 3729 (1997).

[2] C. Urano, M. Nohara, S. Kondo, F. Sakai, H. Takagi, T. Shiraki, and T. Okubo, Phys. Rev. Lett. **85**, 1052 (2000).

[3] V.I. Anisimov, M.A. Korotin, M. Zölfl, T. Pruschke, K. Le Hur, and T.M. Rice, Phys. Rev. Lett. **83**, 364 (1999).

[4] V. Eyert, K.-H. Höck, S. Horn, A. Loidl, and P.S. Riseborough, Europhys. Lett. **46**, 762 (1999).

[5] J. Matsuno, A. Fujimori, and L.F. Mattheiss, Phys. Rev. B **60**, 1607 (1999).

[6] D.J. Singh, P. Blaha, K. Schwarz, and I.I. Mazin, Phys. Rev. B **60**, 16 359 (1999).

[7] R. Liebmann, *Statistical Mechanics of Periodic Frustrated Ising Systems* (Springer, Berlin, 1986).

[8] B. Canals and C. Lacroix, Phys. Rev. Lett. **80**, 2933 (1998).

[9] M. Isoda and S. Mori, J. Phys. Soc. Jpn. **67**, 4022 (1998).

[10] Y. Yamashita and K. Ueda, Phys. Rev. Lett. **85**, 4960 (2000).

[11] A. Koga and N. Kawakami, Phys. Rev. B **63**, 144432 (2001).
[12] H. Tsunetsugu, Phys. Rev. B **65**, 024415 (2001).
[13] H. Tsunetsugu, J. Phys. Soc. Jpn. **70**, 640 (2001).
[14] M. Shiga, K. Fujisawa, and H. Wada, J. Phys. Soc. Jpn. **62**, 1329 (1993).
[15] R. Ballou, E. Leliévre-Berna, and B. Fåk, Phys. Rev. Lett. **76**, 2125 (1996).
[16] See, for example, Y. Kuramoto and Y. Kitaoka, *Dynamics of Heavy Electrons* (Oxford University Press, New York, 2000), and reference therein.
[17] M. Isoda and S. Mori, J. Phys. Soc. Jpn. **69**, 1509 (2000).
[18] S. Fujimoto, Phys. Rev. B **64**, 085102 (2001).
[19] S. Fujimoto, Phys. Rev. Lett. **89**, 226402 (2002).
[20] C. Lacroix, Can. J. Phys. **79**, 1469 (2001).
[21] H. Tsunetsugu, J. Phys. Soc. Jpn. **71**, 1844 (2002).
[22] S. Burdin, D.R. Grempel, and A. Georges, Phys. Rev. B **66**, 045111 (2002).
[23] Y. Yamashita and K. Ueda, Phys. Rev. B **67**, 195107 (2003).
[24] S. Yoda and K. Yamada, Phys. Rev. B **60**, 7886 (1999).
[25] M. Capone, L. Capriotti, F. Becca, and S. Caprara, Phys. Rev. B **63**, 085104 (2001).
[26] T. Kashima and M. Imada, J. Phys. Soc. Jpn. **70**, 3052 (2001).
[27] H. Morita, S. Watanabe, and M. Imada, J. Phys. Soc. Jpn. **71**, 2109 (2002).
[28] Y. Imai and N. Kawakami, Phys. Rev. B **65**, 233103 (2002).
[29] V. Elser, Phys. Rev. Lett. **62**, 2405 (1989).
[30] C. Zeng and V. Elser, Phys. Rev. B **51**, 8318 (1995).
[31] J.T. Chalker and J.F.G. Eastmond, Phys. Rev. B **46**, 14 201 (1992).
[32] F. Mila, Phys. Rev. Lett. **81**, 2356 (1998).
[33] P. Sindzingre, G. Misguich, C. Lhuillier, B. Bernu, L. Pierre, Ch. Waldtmann, and H.-U. Everts, Phys. Rev. Lett. **84**, 2953 (2000).
[34] G. Baym and L.P. Kadanoff, Phys. Rev. **124**, 287 (1961).
[35] G. Baym, Phys. Rev. **127**, 1391 (1962).
[36] N.E. Bickers, D.J. Scalapino, and S.R. White, Phys. Rev. Lett. **62**, 961 (1989).
[37] T. Dahm and L. Tewordt, Phys. Rev. B **52**, 1297 (1995).
[38] M. Langer, J. Schmalian, S. Grabowski, and K.H. Bennemann, Phys. Rev. Lett. **75**, 4508 (1995).
[39] S. Wermbter, Phys. Rev. B **53**, 10 569 (1996).
[40] T. Takimoto and T. Moriya, J. Phys. Soc. Jpn. **66**, 2459 (1997).
[41] R. Arita, S. Onoda, K. Kuroki, and H. Aoki, J. Phys. Soc. Jpn. **69**, 785 (2000).
[42] E.H. Lieb, Phys. Rev. Lett. **62**, 1201 (1989).
[43] H.J. Vidberg and J.W. Serene, J. Low Temp. Phys. **29**, 179 (1977).
[44] G. Kotliar, Phys. Rev. B **37**, 3664 (1988).
[45] I. Affleck and J.B. Marston, Phys. Rev. B **37**, 3774 (1988).
[46] C. Nayak and E. Pivovarov, Phys. Rev. B **66**, 064508 (2002).
[47] E.J.W. Verwey and P.W. Haaymann, Physica **8**, 979 (1941).
[48] A.P. Ramirez, G.P. Espinosa, and A.S. Cooper, Phys. Rev. Lett. **64**, 2070 (1990).
[49] Y.J. Uemura, A. Keren, K. Kojima, L.P. Le, G.M. Luke, W.D. Wu, Y. Ajiro, T. Asano, Y. Kuriyama, M. Mekata, H. Kikuchi, and K. Kakurai, Phys. Rev. Lett. **73**, 3306 (1994).